International Journal of Control, Automation, and Systems 20(7) (2022) 2340-2352
http://dx.doi.org/10.1007/s12555-021-0146-5
ISSN:1598-6446 eISSN:2005-4092
http://www.springer.com/12555

Design of Adaptive RBFNN and Computed-torque Control for Manipulator Joint Considering Friction Modeling

Xiaobin Shen, Kun Zhou, Rui Yu, and Binrui Wang*

Abstract: In this paper, we aim to improve the tracking performance of the manipulator joint system by establishing accurate friction model based on the Stribeck model and the cubic polynomial method. Meanwhile, in view of the established system model, an adaptive Radial Basis Function Neural Network (RBFNN) compensation computed-torque controller is designed for the manipulator joint system. Firstly, we consider the friction modeling process at low- and high- velocity regions to advance the model accuracy, and identify the parameters in the friction model equation offline via the particle swarm optimization (PSO) algorithm. Secondly, an adaptive RBFNN algorithm is developed to analyze the unmodeled dynamics online and introduce it to the computed-torque controller design. After that, we further conduct the stability analysis for the proposed controller based on the Lyapunov stability criterion. Finally, the self-developed manipulator joint platform introduction, the simulation experiment and the contradistinctive experiments are given to illustrate the effectiveness of designed controller.

Keywords: Adaptive control, computed-torque control, friction model, manipulator joint, radial basis function neural network (RBFNN).

1. INTRODUCTION

In recent years, manipulator joints are developing towards modularization and integration, which are widely used in field of industry [1], medical [2,3], human-robot cooperation [4,5], and so on. Therefore, a variety of innovative modular manipulator joints have emerging, which can be composed of different manipulators to complete specific tasks. For example, in [1], the dual-arm manipulator robot was used in a footwear production setting. In [2], the authors developed a robotic spine surgery systems which based on KUKA LBR collaborative robot. In [4], Lorenzo Baccelliere designed a modular robot joint with force feedback and a dual arm robot was built for human-robot interaction experiments. And the paper [5] developed a lightweight robot with the joint contains two encoders and a force sensor, which can perceive the external force from the environment sensitively.

Generally, manipulator joints consist of motors, drivers, sensors and reducers. The reducer has serious nonlinear friction, which will affect control accuracy [6] and increase control difficulty. The nonlinear friction can be divided into the dynamic friction and the static friction, and many models have been established in the literatures, such as the Coulomb friction model [7,8], Stribeck model [9,10], Dahl model [11] and LuGre model [12,13]. Based on the above modeling methods, many research works have developed the different friction models by considering some discrepant influence factors. For example, the paper [14] discussed the friction model with the Stribeck model and used the Gaussian compensation term to restrain the reversal chattering. The work [15] established a dynamic model based on the LuGre model for the clearance joint, and it is proved that the proposed model is superior to the coulomb friction model. In addition, the temperature influence also was considered in [16], the authors established a friction model with temperature correction for the robot joints. Therefore, it is difficult to establish an accurate model considering different effects.

The unknown parameters in the nonlinear friction model have also attracted the attention of many researchers. Consequently, many parameter identification algorithms have been used in the establishment of nonlinear friction models, such as least square method, genetic algorithm, and particle swarm optimization algorithm. In [17], the simulated annealing method was introduced in the genetic algorithm to identify the friction model affected by vibration and collision. The genetic method and

Manuscript received February 23, 2021; revised May 27, 2021 and August 1, 2021; accepted September 16, 2021. Recommended by Associate Editor Ning Sun under the direction of Editor Kyoung Kwan Ahn. This work was supported by the National Key Research and Development Project of China (Grant No. 2018YFB2101004, 2018YFC0809204).

Xiaobin Shen, Kun Zhou, and Binrui Wang are with the College of Mechanical and Electrical Engineering, China Jiliang University, Hangzhou, Zhejiang 310018, China (e-mails: {15957152941, 13488950521, wangbrpaper}@163.com). Rui Yu is with the School of Electronic Information and Engineering, Tongji University, Shanghai 201804, China (e-mail: fisherrui@163.com).
* Corresponding author.

PSO method were combined in [18] to identify the nonlinear friction model, and a high identification accuracy was achieved. Besides, the authors compared the dynamic PSO algorithm with the artificial bee colony algorithm in [19], and proved that the PSO algorithm has higher identification correction.

For the research of manipulator joint trajectory tracking, many control algorithms have been applied to the manipulator joint system, such as PID control, computed-torque control [20,21], model predictive control [22], neural networks algorithm [23–25], and fuzzy control [26–29]. For instance, Jiang *et al*. [25] designed a RBFNN compensator based on the computed-torque controller to estimate and compensate the friction torque online, but the nonlinear friction model of the joint was not considered. In [29], the researchers used the fuzzy PID algorithm for the robot dynamics with Stribeck friction model. However, the fuzzy control must depend on the experience of users, which is tough to design. Besides, adaptive control is also widely used in manipulator systems [30–32] for uncertain items. Sun *et al*. [30] proposed a reduced adaptive fuzzy decoupling control method for exoskeleton system, and the adaptive control was considered to approximate the coupling parameters in the work.

Motivated by the manipulator joint works mentioned before, the aim of this paper is to achieve the high-precision trajectory tracking performance for the manipulator joint system. To carry out this goal, we firstly establish an accurate friction model based on the Stribeck model and the cubic polynomial method, which can divide friction modeling process into low- and high- velocity regions to advance the model accuracy. Then, refer to [18,19], PSO algorithm is chosen to identify the unknown parameters in the friction model equation offline, due to its high identification accuracy. Under the comparison of different control methods, we develop a computed-torque control algorithm with the adaptive RBFNN method for the manipulator joint dynamic equation which contains the uncertain items. The adaptive neural network algorithm is considered to estimate the unknown items online, which can effectively enhance the system tracking accuracy. Moreover, we demonstrate the effectiveness of the established model and the proposed algorithm through the simulation experiments and the comparative experiment on the self-developed manipulator joint platform. The contributions of this paper can be summarized as follows:

1) A multi-stage Stribeck friction model based on cubic polynomial is established to improve the accuracy of the friction model in a large velocity range.
2) We consider the unmodeled dynamic terms in the manipulator joint model, and employ the adaptive neural network algorithm to estimate and solve it online.
3) An adaptive RBFNN computed-torque controller has been designed for the proposed manipulator joint dynamic model, and its good control effect is verified by simulation and comparative experiments based on the self-developed platform.

This paper is organized as follows: The dynamic model and friction model of the robot joint system will be carried out in Section 2. In Section 3, the adaptive RBFNN computed-torque controller is designed for the established dynamic model. And the self-developed manipulator joint platform introduction, the simulation experiment and the comparative experiments in Section 4. Finally, the conclusion and future works are shown in Section 5.

2. MODELING

2.1. Dynamic model of manipulator

For an multi-joint manipulator, its dynamic equation can be expressed as

$$\boldsymbol{M}(\boldsymbol{q})\ddot{\boldsymbol{q}}+\boldsymbol{C}(\boldsymbol{q},\dot{\boldsymbol{q}})\dot{\boldsymbol{q}}+\boldsymbol{G}(\boldsymbol{q})=\boldsymbol{\tau}, \tag{1}$$

where $\boldsymbol{\tau}$ is joint turque of the manipulator, $\boldsymbol{M}(\boldsymbol{q})$ is the equivalent inertia term, $\boldsymbol{C}(\boldsymbol{q},\dot{\boldsymbol{q}})$ is the contribution of the centripetal and Coriolis forces, $\boldsymbol{G}(\boldsymbol{q})$ is the contribution of gravity at the output, $\boldsymbol{q}$, $\dot{\boldsymbol{q}}$, $\ddot{\boldsymbol{q}}$ denote the position, velocity and acceleration.

When considering the joint friction model of the manipulator, the dynamic model of the manipulator can be rewritten as

$$\boldsymbol{M}(\boldsymbol{q})\ddot{\boldsymbol{q}}+\boldsymbol{C}(\boldsymbol{q},\dot{\boldsymbol{q}})\dot{\boldsymbol{q}}+\boldsymbol{G}(\boldsymbol{q})+\boldsymbol{\tau}_{\mathrm{jf}}=\boldsymbol{\tau}, \tag{2}$$

where $\boldsymbol{\tau}_{\mathrm{jf}}$ denotes the friction model of manipulator joint.

The unmodeled dynamics in (2), such as friction model error and dynamic model error, can be inserted into the dynamic model of the manipulator joint by changing (2) to

$$\boldsymbol{M}_0(\boldsymbol{q})\ddot{\boldsymbol{q}}+\boldsymbol{C}_0(\boldsymbol{q},\dot{\boldsymbol{q}})\dot{\boldsymbol{q}}+\boldsymbol{G}_0(\boldsymbol{q})+\boldsymbol{\tau}_{\mathrm{jf0}}-\boldsymbol{f}(\cdot)=\boldsymbol{\tau} \tag{3}$$

where

$$\begin{aligned}
&\boldsymbol{f}(\cdot)=\Delta\boldsymbol{M}\ddot{\boldsymbol{q}}+\Delta\boldsymbol{C}\dot{\boldsymbol{q}}+\Delta\boldsymbol{G}+\boldsymbol{\tau}_{\mathrm{jf}},\\
&\boldsymbol{M}(\boldsymbol{q})=\boldsymbol{M}_0(\boldsymbol{q})-\Delta\boldsymbol{M},\\
&\boldsymbol{C}(\boldsymbol{q},\dot{\boldsymbol{q}})=\boldsymbol{C}_0(\boldsymbol{q},\dot{\boldsymbol{q}})-\Delta\boldsymbol{C},\\
&\boldsymbol{G}(\boldsymbol{q})=\boldsymbol{G}_0(\boldsymbol{q})-\Delta\boldsymbol{G},\\
&\boldsymbol{\tau}_{\mathrm{jf}}=\boldsymbol{\tau}_{\mathrm{jf0}}-\Delta\boldsymbol{\tau}_{\mathrm{jf}},
\end{aligned}$$

where $\boldsymbol{M}_0(\boldsymbol{q})$, $\boldsymbol{C}_0(\boldsymbol{q},\dot{\boldsymbol{q}})$ and $\boldsymbol{G}_0(\boldsymbol{q})$ can be obtained by using a computer-aided designed (CAD) software, $\boldsymbol{\tau}_{\mathrm{jf0}}$ can be obtained by friction modeling, $\Delta\boldsymbol{M}$, $\Delta\boldsymbol{C}$, $\Delta\boldsymbol{G}$ and $\Delta\boldsymbol{\tau}_{\mathrm{jf}}$ are terms referring to the error of the system, $\boldsymbol{f}(\cdot)$ is the unmodeled dynamics of the system.

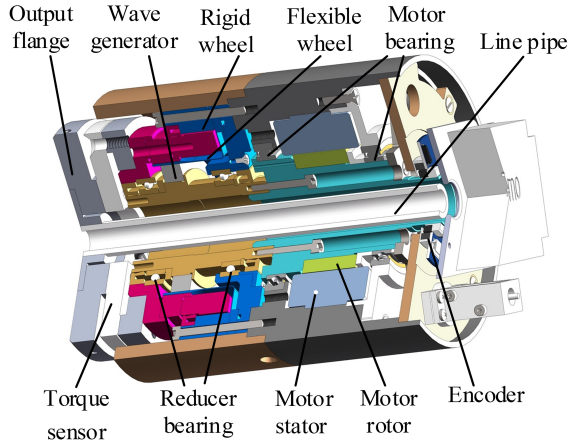

Fig. 1. Joint model diagram.

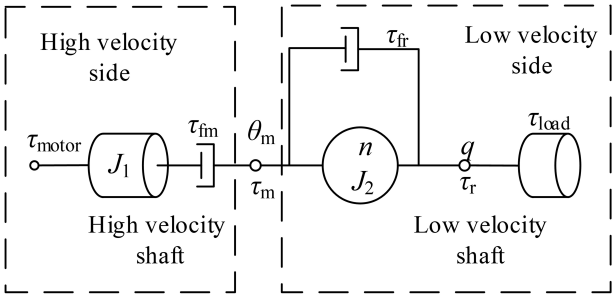

Fig. 2. Joint transmission diagram.

2.2. Dynamic model of manipulator joint

In this subsection, we will develop the dynamic model for the manipulator joint based on the dynamic model of manipulator. The 3D model of the manipulator joint is given in Fig. 1. And the schematic diagram of the joint transmission chain is presented in Fig. 2.

In Fig. 2, τ_{motor} is the electromagnetic torque of motor, J_1 and J_2 are the momentum of inertia of the high-velocity and low- velocity shafts, respectively, τ_{fm} and τ_{fr} mean the friction torque at high-velocity and low-velocity sides, respectively, θ_m stands for the position of the high-velocity side, τ_m means output torque at high-velocity side; n is the reduction ratio, τ_r means the output torque at the low-velocity side.

Through the analysis of Fig. 2, the electromagnetic torque generated by the DC servo motor can be expressed as

$$\tau_{motor} = K_m i, \tag{4}$$

where K_m denotes the motor torque constant, and i denotes the motor current.

The dynamic equation of high-velocity shaft can be expressed as

$$\tau_m = \tau_{motor} - \tau_{fm} - J_1 \ddot{\theta}_m. \tag{5}$$

Meanwhile, the dynamic equation of high-velocity shaft can be obtained as

$$n\tau_m = \tau_r + \tau_{fr} + J_2 \ddot{q}. \tag{6}$$

Assuming the stiffness of the harmonic reducer is sufficiently large and the deformation of the harmonic reducer could be neglected, the relationship between θ_m and q is

$$q = \frac{\theta_m}{n}. \tag{7}$$

Combining (2) and (4)-(7), the dynamic model of the robot joint is defined as

$$n\tau_{motor} = J\ddot{q} + n\tau_f + \tau_r + f(\cdot), \tag{8}$$

where $J = n^2 J_1 + J_2$ denotes the equivalent momentum of inertia on the low-velocity side, and $\tau_f = \tau_{fm} + \tau_{fr}/n$ denotes the equivalent friction torque on the high-velocity side.

Remark 1: The torque balance equations with low velocity shaft or high velocity shaft as reference can be converted to each other. However, in order to unify in the subsequent calculation process, the low-velocity axis will only be considered for the manipulator dynamic model.

Due to the importance of the nonlinear friction part in the joint, we will consider the friction model for the manipulator joint in the next subsection.

2.3. Friction model of manipulator joint

In this subsection, the friction characteristics of the manipulator joint will be modeled. Firstly, we can obtain the relationship between velocity with friction torque in Fig. 3, through the data measurement and the following equations.

From (4) and (8), the τ_f can be obtained as follows:

$$\tau_f = -\frac{1}{n}[J\ddot{q} + \tau_r + f(\cdot)] + K_m i. \tag{9}$$

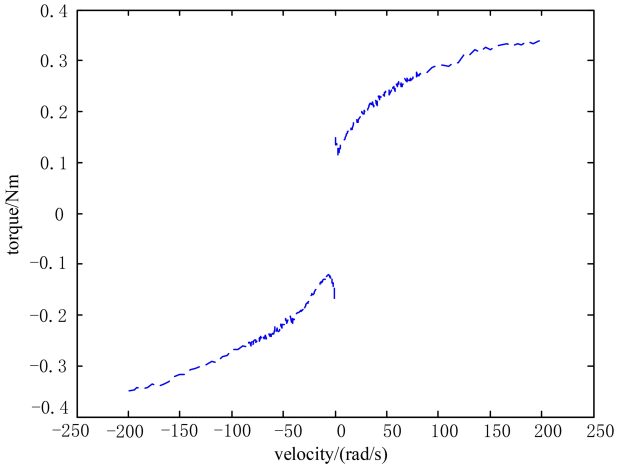

Fig. 3. Velocity-friction torque diagram.

Because the joint friction torque can be regarded as the electromagnetic torque generated by the motor under no load and assume $f(\cdot) = 0$. Equation (9) can be rewritten as

$$\tau_{\mathrm{f}} = K_{\mathrm{m}} i. \tag{10}$$

Remark 2: For convenience, we only consider the effect of velocity during the friction modeling in this paper. However, other influence factors also can be considered in future works, such as temperature, position and external load.

Remark 3: The relationship curve in Fig. 3 is obtained through the self-develop manipulator joint platform, and is familiar with the results from other brand manipulator joint and in [33]. Thus, the relationship in Fig. 3 can be regarded as a typical velocity-friction torque relationship for modeling.

Then, it is obvious that the low-velocity segment in Fig. 3 fits to the Stribeck model. However, the friction curve is not completely in conformity with the Stribeck model when the velocity increase, especially in high-velocity segment.

Consequently, a multistage friction model is proposed in this paper, in which the Stribeck friction model and a lower-order cubic polynomial are applied in the low- and high-velocity segments, respectively. The friction model τ_{f} for velocity v can be expressed as

$$\begin{cases} \varphi^{-}(v) = f_{\mathrm{a0}}^{-} + f_{\mathrm{a1}}^{-} v + f_{\mathrm{a2}}^{-} v^2 + f_{\mathrm{a3}}^{-} v^3, \ v_{\max}^{-} \le v < v^{-}, \\ \tau_{\mathrm{fs}}^{-}(v) = -\tau_{\mathrm{c}}^{-} - (\tau_{\mathrm{s}}^{-} - \tau_{\mathrm{c}}^{-}) e^{-\frac{v}{\omega_{\mathrm{s}}^{-}}^2} + \tau_{v}^{-} v, \ v^{-} \le v < 0, \\ \tau_{\mathrm{fs}}^{+}(v) = \tau_{\mathrm{c}}^{+} + (\tau_{\mathrm{s}}^{+} - \tau_{\mathrm{c}}^{+}) e^{-\frac{v}{\omega_{\mathrm{s}}^{+}}^2} + \tau_{v}^{+} v, \ 0 \le v \le v^{+}, \\ \varphi^{+}(v) = f_{\mathrm{a0}}^{+} + f_{\mathrm{a1}}^{+} v + f_{\mathrm{a2}}^{+} v^2 + f_{\mathrm{a3}}^{+} v^3, \ v^{+} < v \le v_{\max}^{+}, \end{cases} \tag{11}$$

where $v_{\max}^{-}$ and v^{-} denote the maximum and critical rotation velocity of motor in the negative direction, $v_{\max}^{+}$ and v^{+} denote the maximum and critical rotation velocity of motor in the positive direction, f_{a0}^{-}, f_{a1}^{-}, f_{a2}^{-}, f_{a3}^{-} and f_{a0}^{+}, f_{a1}^{+}, f_{a2}^{+}, f_{a3}^{+} denote the coefficients of the cubic polynomial, τ_{c}^{-} and τ_{c}^{+} denote the Coulomb friction, τ_{s}^{-} and τ_{s}^{+} mean static friction torque, τ_{v}^{-} and τ_{v}^{+} stand for the coefficient of viscous friction, ω_{s}^{-} and ω_{s}^{+} denote feature velocity.

2.4. Parameters identification of friction model

The developed friction model (11) is a nonlinear multi-segmented model, which is composed of parameters that need to be identified. Refer to [22–24], we choose the PSO algorithm to identify the unknown parameters, because it has the faster convergence speed, no codon, less internal parameters and engineering application value. The flow chart of the PSO algorithm is presented in Fig. 4. Firstly,

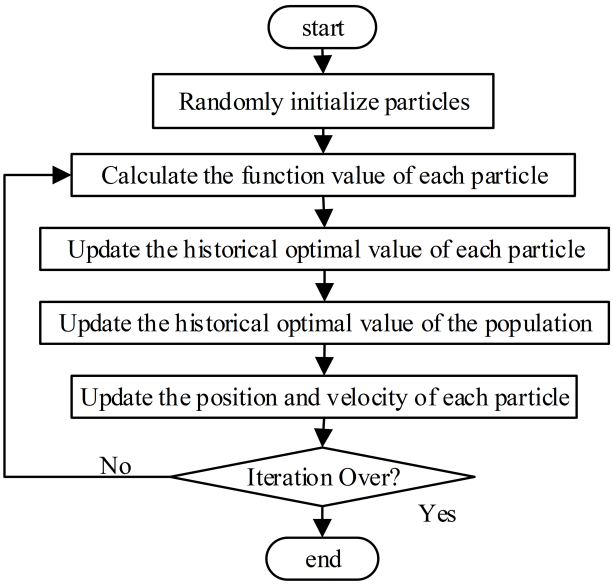

Fig. 4. Flow chart of PSO.

the fitness function (E) of the PSO, which contains unknown parameters in the friction model (11), can be defined as

$$E = \sum_{c=0}^{S} \left[\tau_{\mathrm{f}}(v_c) - \tau_{\mathrm{af}}(v_{\mathrm{c}})\right]^2, \tag{12}$$

where v_{c} is the sample velocity, S denotes the total number of samples in the experiment, $\tau_{\mathrm{f}}(v_{\mathrm{c}})$ is the friction torque which can be calculated by (11), $\tau_{\mathrm{af}}(v_{\mathrm{c}})$ is the friction torque which is sampled from the manipulator joint. Noticeably, when the E in (12) reaches to the minimum point, we can obtain the optimal values of the identified parameters.

3. CONTROLLER DESIGN

In view of the dynamic equation, we will design and analyse the controller for the manipulator system in this section.

Let $\boldsymbol{q}_{\mathrm{d}}$ be the desired trajectory of the manipulator joints, the actual tracking error $\boldsymbol{e}$ can be defined as

$$\boldsymbol{e} = \boldsymbol{q} - \boldsymbol{q}_{\mathrm{d}}. \tag{13}$$

Based on the computed-torque control scheme [34] and the manipulator model (3), and the RBFNN is used to estimate the $\boldsymbol{f}(\cdot)$, the controller of the manipulator can be designed as

$$\begin{aligned} \boldsymbol{\tau}_{\mathrm{out}} &= \boldsymbol{M}_0(\boldsymbol{q})(\ddot{\boldsymbol{q}}_{\mathrm{d}} - \boldsymbol{k}_{\mathrm{v}}\dot{\boldsymbol{e}} - \boldsymbol{k}_{\mathrm{p}}\boldsymbol{e}) + \boldsymbol{C}_0(\boldsymbol{q},\dot{\boldsymbol{q}})\dot{\boldsymbol{q}} \\ &\quad + \boldsymbol{G}_0(\boldsymbol{q}) + \boldsymbol{\tau}_{\mathrm{jf0}} - \hat{\boldsymbol{f}}(x), \\ \hat{\boldsymbol{f}}(\boldsymbol{x}) &= \hat{\boldsymbol{w}}^{\mathrm{T}}\boldsymbol{h}(\boldsymbol{x}), \end{aligned} \tag{14}$$

where $\boldsymbol{\tau}_{\text{out}}$ is the output torque of the controller, $\boldsymbol{k}_{\text{v}}$ and $\boldsymbol{k}_{\text{p}}$ are the symmetric positive definite matrices, $\hat{\boldsymbol{f}}(\cdot)$ is the estimation of the $\boldsymbol{f}(\cdot)$, $\hat{\boldsymbol{w}}$ and $\boldsymbol{x}$ are the estimated weights and the input vector of the neural network, $\boldsymbol{h}(\boldsymbol{x}) = \exp(-|\boldsymbol{x} - \boldsymbol{c}^2|/(2\boldsymbol{b}^2))$ is radial basis function with the width vector $\boldsymbol{b}$ and center vector $\boldsymbol{c}$.

When the modeling error and external disturbance in the system are not considered, therefore, $\boldsymbol{f}(\cdot) = 0$, the error dynamics can be expressed as

$$\ddot{\boldsymbol{e}}_{\text{d}} + \boldsymbol{k}_{\text{v}}\dot{\boldsymbol{e}} + \boldsymbol{k}_{\text{p}}\boldsymbol{e} = \boldsymbol{0}. \tag{15}$$

In this ideal situation, $(\dot{\boldsymbol{e}}, \boldsymbol{e}) = (\boldsymbol{0}, \boldsymbol{0})$ is a balanced point of the global asymptotic stability as long as $\boldsymbol{k}_{\text{v}}$ and $\boldsymbol{k}_{\text{p}}$ are symmetric positive definite matrices. Therefore, the computed-torque controller avoids the calculation of $\ddot{\boldsymbol{q}}$, and only $\boldsymbol{q}$ and $\dot{\boldsymbol{q}}$ need to be concerned.

At most time, $\boldsymbol{f}(\cdot)$ always exists and is unknown, thus, by combining (3) and (14), the error equation can be rewritten as

$$\ddot{\boldsymbol{e}} + \boldsymbol{k}_{\text{v}}\dot{\boldsymbol{e}} + \boldsymbol{k}_{\text{p}}\boldsymbol{e} = \boldsymbol{M}_0^{-1}(\boldsymbol{q})\left[\boldsymbol{f}(\cdot) - \hat{\boldsymbol{f}}(x)\right]. \tag{16}$$

Let the neural network input $\boldsymbol{x} = [\boldsymbol{e}\ \dot{\boldsymbol{e}}]^{\text{T}}$ as the state variable, (16) can be modified to

$$\dot{\boldsymbol{x}} = \boldsymbol{A}\boldsymbol{x} + \boldsymbol{B}\left[\boldsymbol{f}(\cdot) - \hat{\boldsymbol{f}}(\boldsymbol{x})\right], \tag{17}$$

where $\boldsymbol{A} = \begin{bmatrix} 0 & \boldsymbol{I} \\ -\boldsymbol{k}_{\text{p}} & -\boldsymbol{k}_{\text{v}} \end{bmatrix}$, $B = \begin{bmatrix} \boldsymbol{0} \\ \boldsymbol{M}_0^{-1}(\boldsymbol{q}) \end{bmatrix}$.

Moreover, the RBFNN approximation error $\boldsymbol{\varepsilon}$ is defined as

$$\boldsymbol{\varepsilon} = \boldsymbol{f}(\cdot) - \boldsymbol{f}^*(\boldsymbol{x}) \tag{18}$$

where $\boldsymbol{f}^*(\boldsymbol{x}) = \boldsymbol{w}^{*\text{T}}\boldsymbol{h}(\boldsymbol{x})$ is the optimal output with the optimal weight $\boldsymbol{w}^*$.

Assuming that $\boldsymbol{\varepsilon}$ is bounded, the maximum output error $\boldsymbol{\varepsilon}_0$ of RRFNN can be expressed as

$$\boldsymbol{\varepsilon}_0 = \sup\|\boldsymbol{f}(\cdot) - \boldsymbol{f}^*(\boldsymbol{x})\|. \tag{19}$$

Therefore, the error equation of the entire system in state-space form is obtained as

$$\dot{\boldsymbol{x}} = \boldsymbol{A}\boldsymbol{x} + \boldsymbol{B}\left[\boldsymbol{\varepsilon} - \tilde{\boldsymbol{w}}^{\text{T}}\boldsymbol{h}(\boldsymbol{x})\right], \tag{20}$$

where $\tilde{\boldsymbol{w}} = \hat{\boldsymbol{w}} - \boldsymbol{w}^*$ denotes weight error.

Meanwhile, the Lyapunov equation can be expressed as

$$\boldsymbol{P}\boldsymbol{A} + \boldsymbol{A}^{\text{T}}\boldsymbol{P} = -\boldsymbol{Q}, \tag{21}$$

where $\boldsymbol{P}$ and $\boldsymbol{Q}$ are the symmetric positive definite matrices.

Then, we use the Lyapunov method to derive the adaptation law and prove the stability of the system. The Lyapunov function V is designed as

$$V = \frac{1}{2}\boldsymbol{x}^{\text{T}}\boldsymbol{P}\boldsymbol{x} + \frac{1}{2\beta}\|\tilde{\boldsymbol{w}}\|^2, \tag{22}$$

where $\beta > 0$. Thus, V is a positive definite function.

The derivative $\dot{V}$ can be obtained as

$$\begin{aligned}\dot{V} = &-\frac{1}{2}\boldsymbol{x}^{\text{T}}\boldsymbol{Q}\boldsymbol{x} + \frac{1}{\beta}tr(-\beta\boldsymbol{B}^{\text{T}}\boldsymbol{P}\boldsymbol{x}\boldsymbol{h}^{\text{T}}(\boldsymbol{x})\tilde{\boldsymbol{w}} + \dot{\hat{\boldsymbol{w}}}^{\text{T}}\tilde{\boldsymbol{w}}) \\ &+ \boldsymbol{\varepsilon}^{T}\boldsymbol{B}^{\text{T}}\boldsymbol{P}\boldsymbol{x},\end{aligned} \tag{23}$$

where $tr(\cdot)$ is the trace of the matrix.

Let the adaptive law as

$$\dot{\hat{\boldsymbol{w}}} = \beta\boldsymbol{h}(\boldsymbol{x})\boldsymbol{x}^{\text{T}}\boldsymbol{P}\boldsymbol{B}. \tag{24}$$

Theorem 1: With adaptive RBFNN compensation computed-torque controller including the control law (14) and the adaptation law (24), the manipulator system is stable, and $(\dot{\boldsymbol{e}}, \boldsymbol{e}) \to (\boldsymbol{0}, \boldsymbol{0})$ as $t \to \infty$.

Proof: Substituting (24) into (23) can yield

$$\dot{V} = -\frac{1}{2}\boldsymbol{x}^{\text{T}}\boldsymbol{Q}\boldsymbol{x} + \boldsymbol{\varepsilon}^{\text{T}}\boldsymbol{B}^{\text{T}}\boldsymbol{P}\boldsymbol{x}. \tag{25}$$

Considering (25) and the principle of inequality, the following inequality is obtained

$$\begin{aligned}\dot{V} \le &-\frac{1}{2}\|\boldsymbol{x}\|[\lambda_{\min}(\boldsymbol{Q})\|\boldsymbol{x}\| \\ &- 2\|\boldsymbol{\varepsilon}_0\|\|\boldsymbol{M}_0^{-1}(\boldsymbol{q})\|\lambda_{\max}(\boldsymbol{P})],\end{aligned} \tag{26}$$

where $\lambda_{\min}(\boldsymbol{Q})$ is the minimum eigenvalue of $\boldsymbol{Q}$, and $\lambda_{\max}(\boldsymbol{P})$ is the maximum eigenvalue of $\boldsymbol{P}$.

Then, the following inequality (27) needs to be proved to be true, which is expressed as

$$\lambda_{\min}(\boldsymbol{Q})\|\boldsymbol{x}\| - 2\|\boldsymbol{\varepsilon}_0\|\|\boldsymbol{M}_0^{-1}(\boldsymbol{q})\|\lambda_{\max}(\boldsymbol{P}) \le 0. \tag{27}$$

Inequality (27) can be rewritten as

$$\lambda_{\min}(\boldsymbol{Q}) \ge \frac{2\|\boldsymbol{M}_0^{-1}(\boldsymbol{q})\|\lambda_{\max}(\boldsymbol{P})}{\|\boldsymbol{x}\|}\|\boldsymbol{\varepsilon}_0\|. \tag{28}$$

In inequality (28), $\boldsymbol{M}_0(\boldsymbol{q})$ is a constant parameter, $\boldsymbol{Q}$ and $\boldsymbol{P}$ are the constant parameters of the controller. And $\boldsymbol{\varepsilon}_0$ is the boundary value of $\boldsymbol{\varepsilon}$, so $\|\boldsymbol{x}\|_{\max}$ is obtained with $\boldsymbol{\varepsilon} = \boldsymbol{\varepsilon}_0$. Therefore, the values of $\boldsymbol{Q}$ and $\boldsymbol{P}$ can always be found to ensure inequality (28) to be true and $\dot{V} \le 0$.

Through above proof, we can know $(\dot{\boldsymbol{e}}, \boldsymbol{e}) \to (\boldsymbol{0}, \boldsymbol{0})$ as $t \to \infty$ when the adaptive law (25) is used. Thus, the stability of the manipulator system can be ensured.

Finally, the complete controller can be expressed as

$$\begin{aligned}&\boldsymbol{\tau}_{\text{out}} = \boldsymbol{M}_0(\boldsymbol{q})(\ddot{\boldsymbol{q}}_{\text{d}} - \boldsymbol{k}_{\text{v}}\dot{\boldsymbol{e}} - \boldsymbol{k}_{\text{p}}\boldsymbol{e}) + \boldsymbol{C}_0(\boldsymbol{q}, \dot{\boldsymbol{q}})\dot{\boldsymbol{q}} \\ &\qquad + \boldsymbol{G}_0(\boldsymbol{q}) + \boldsymbol{\tau}_{\text{jf0}} - \hat{\boldsymbol{f}}(\boldsymbol{x}), \\ &\hat{\boldsymbol{f}}(x) = \hat{\boldsymbol{w}}^{\text{T}}\boldsymbol{h}(\boldsymbol{x}), \\ &\dot{\hat{\boldsymbol{w}}} = \beta\boldsymbol{h}(\boldsymbol{x})\boldsymbol{x}^{\text{T}}\boldsymbol{P}\boldsymbol{B}.\end{aligned} \tag{29}$$

The block diagram of the designed adaptive RBFNN compensation computed-torque controller is presented in Fig. 5.

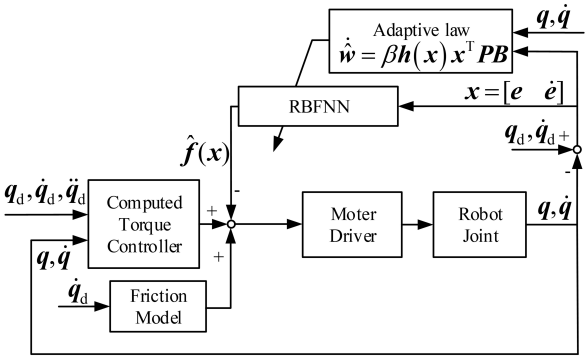

Fig. 5. Block diagram of the control system.

Besides, inequality (28) can also be rewritten as

$$\|\boldsymbol{x}\| \geq \frac{2\|\boldsymbol{M}_0^{-1}(\boldsymbol{q})\|\lambda_{\max}(\boldsymbol{P})}{\lambda_{\min}(\boldsymbol{Q})}\|\boldsymbol{\varepsilon}_0\|. \tag{30}$$

In inequality (30), as the eigenvalue of $\boldsymbol{Q}$ increases or the eigenvalue of $\boldsymbol{P}$ decreases, the system converges faster and its accuracy is improved.

4. EXPERIMENT STUDY

4.1. Platform introduction and parameter identification

In this subsection, the self-developed manipulator joint platform is presented in Fig. 6, and the system parameters will be given as follows:

Firstly, the main component models used in the manipulator joint are given in Table 1, and the manipulator joint's parameters are shown in Table 2.

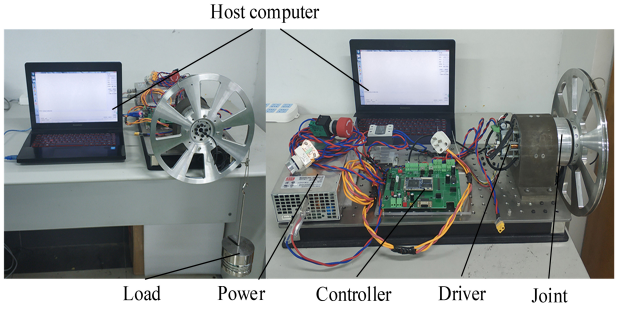

Fig. 6. Experimental equipment diagram.

Table 1. The models of the main parts.

Item	Model
Motor	TBM7615A
Reducer	LHSG-20-CL-120
Encoder	MBS
Driver	G-MOLWHI20/100SE

Table 2. Robot joint parameters.

Item	Parameter
Rated torque (Nm)	60
Rated velocity (r/min)	33
Reduction ratio	$n = 121$
Inertia (Kg·m^2)	$J = 2.1$

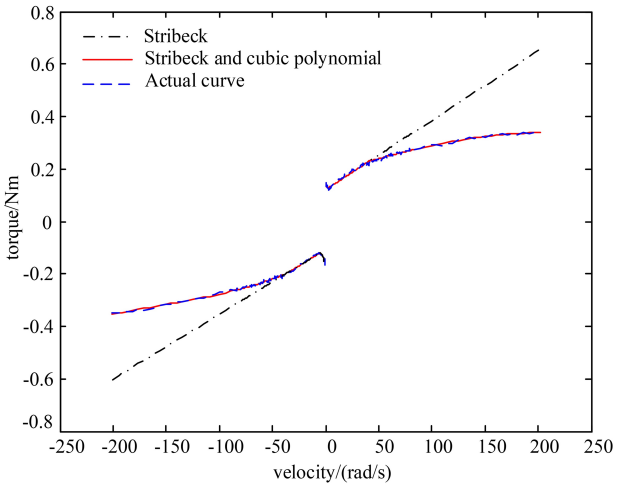

(a) Fitting comparison.

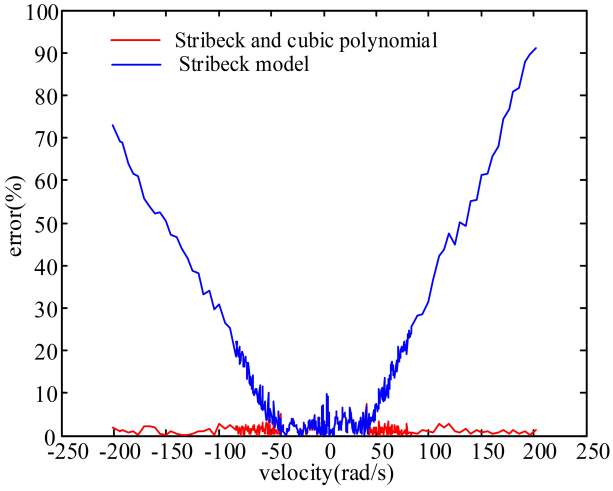

(b) Fitting error.

Fig. 7. Parameter optimization results.

Then, identify the parameters of the friction model based on the PSO algorithm, and some coefficients are set as follows:

$\boldsymbol{C}_0(\boldsymbol{q}, \dot{\boldsymbol{q}}) = \boldsymbol{G}(q) = 0$, $S = 225$, $v_{\max}^- = -200$, $v_{\max}^+ = 200$, $v^- = -40$, $v^+ = 40$, and the number of particles and iterations are 1000 and 5000, respectively.

The results of fitting comparison and fitting error are shown in Fig. 7, and the results of parameter identification are presented in Table 3.

Table 3. Friction model parameters.

Item	Positive direction	Negative direction
τ_c	0.11985	0.1063
τ_s	0.14537	0.1575
ω	1.2301	2.887
τ_v	0.0026518	0.002475
$\boldsymbol{f}_{a3}$	-7.6969×10^{-9}	2.1182×10^{-8}
$\boldsymbol{f}_{a2}$	-6.5261×10^{-7}	1×10^{-5}
$\boldsymbol{f}_{a1}$	0.0012298	0.0022866
$\boldsymbol{f}_{a0}$	0.17995	−0.1272

The root-mean-square error (RMSE) is introduced to reflect the deviation between the real value and the fitting value of the joint friction model. The smaller the RMSE, the higher the fitting accuracy, and the specific calculation formula is as follows:

$$RMSE = \sqrt{\frac{1}{S}E}. \tag{31}$$

Fig. 7(a) presents the fitting diagram only using the Stribeck friction model and its RMSE is 0.0632 Nm. Meanwhile, it also presents the friction model fitting diagram with proposed model and its RMSE is 0.0046 Nm. Fig. 7 and the RMSE value demonstrate that the proposed friction model can more accurately represent the static friction characteristics at the joints compared with the Stribeck model only.

Taking the identified parameters into the model equation (11), the calculated value of joint friction torque can be obtained. By comparing with the actual friction torque , we can obtain the error diagram as shown in Fig. 7(b). The fitting error is less than 10% when fit with Stribeck and cubic polynomial, which is far less than fitting with Stribeck model only. Thus, the effectiveness of the proposed joint friction model can be verified.

Finally, the related parameters in neural network and controller will be given as follows:

The number of neurons in the hidden layer are 15 and the center vector is defined as

$$\boldsymbol{c} = \begin{bmatrix} -\boldsymbol{c}_p & 0 & \boldsymbol{c}_p \end{bmatrix},$$

where

$$\boldsymbol{c}_p = 10^{-2}\times\begin{bmatrix} -5 & -3 & -1 & -0.8 & -0.4 & -0.1 & -0.05 \\ -5 & -3 & -1 & -0.8 & -0.4 & -0.1 & -0.05 \end{bmatrix}.$$

The radial basis function width is constructed as

$$\boldsymbol{b} = \begin{bmatrix} 5 & 5 & 5 & 5 & 5 & 5 & 5 & 5 & 5 & 5 & 5 & 5 & 5 & 5 & 5 \end{bmatrix}.$$

Here, the initial value of the neural network weight is selected as 0.01. The other parameters are selected as $\beta = 80$, $k_p = 784$, $k_v = 56$. Note that, at the initial moment, the joint is stationary, at the origin (position zero) and no load is applied to it.

Remark 4: The parameters in the neural network design are determined by simulation and experiments. Then, for the faster convergence, we choose a bigger eigenvalue of $\boldsymbol{Q}$ and a smaller eigenvalue of $\boldsymbol{P}$. Besides, because the established dynamic model still has some errors, the parameter $\boldsymbol{Q}$ designed in simulation and experiment are different, namely $\boldsymbol{Q} = 2500\,\boldsymbol{I}$ and $\boldsymbol{Q} = 1800\,\boldsymbol{I}$, where $\boldsymbol{I}$ is the two dimensional identity matrix.

4.2. Neural network simulation

Due to the limitation of the experimental platform such as memory size and running speed of the microcontroller unit (MCU), we cannot obtain the specific data in the neural network online learning process through platform experiments. Therefore, we design the following simulation experiment to demonstrate the variations in neural network learning.

We set the $0.35\sin(0.2\pi t)$ as the target trajectory, and set 10% as the friction torque error (10% is the maximum calculation error of friction model).

The simulation results are shown in Fig. 8. The inputs of the neural network are shown in Fig. 8(a), which are also the position error and velocity error of the manipulator joint. It shows that the errors are bounded and tending to zero with continuously learning. Besides, the position error in Fig. 8(a) is less than ±0.002 rad, and which is less than the error in [25]. Therefore, this comparison can illustrate that the friction model we have established can improve the control precision effectively. Fig. 8(b) is the comparison result of estimated model error by neural network method with the theoretical value, and it shows that the two tend to be consistent. Figs. 8(c) and 8(d) are the part of weights of the neural network and hidden layer outputs respectively. We know that the weights of the neural network tend to be fixed after learning.

4.3. Comparative platform experiments

In this subsection, we will design some comparative experiments on the self-developed manipulator joint platform to illustrate the effectiveness and superiority of the proposed model and algorithm.

Firstly, we design a set of comparative experiments about whether there is a friction model to compare the effect of joint tracking. The results including tracking curve and RBFNN output curve are shown in Figs. 9 and 10, and the error comparison curves are given in Fig. 11. Besides, Table 4 also demonstrates the specific error range after 75 s for two cases.

From Figs. 10 and 11, we can acquire that the established friction model can effectively decrease the tracking error and the output of RBFNN, especially near the zero velocity of the trajectory.

Secondly, we vary the frequency and amplitude of the target trajectory in the experiment to see how they affect the results. Fig. 12 shows the experiments of chang-

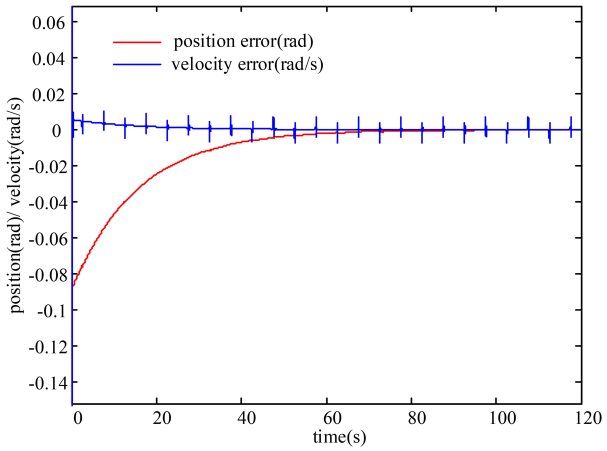

(a) Neural network input.

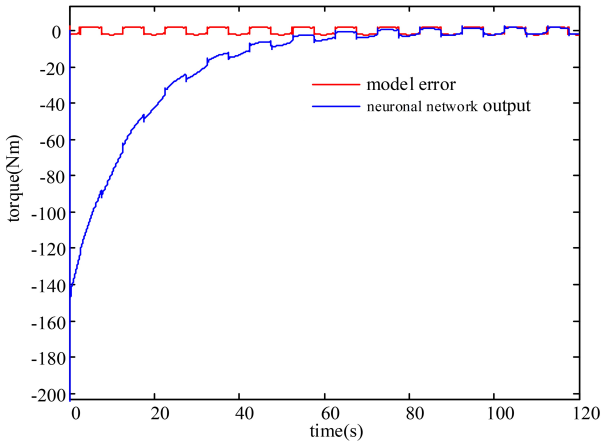

(b) Neural network output.

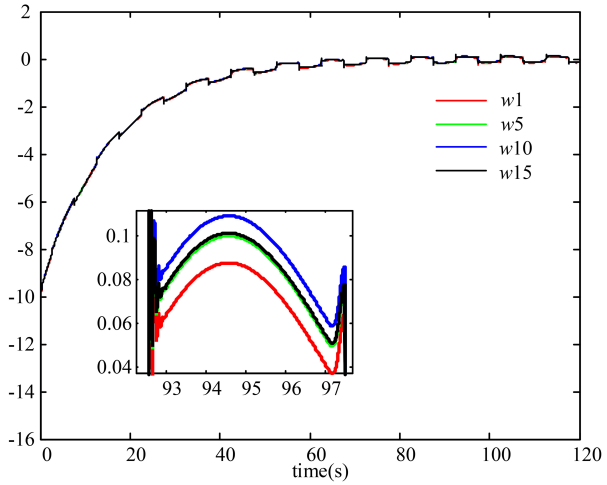

(c) Neural network weight.

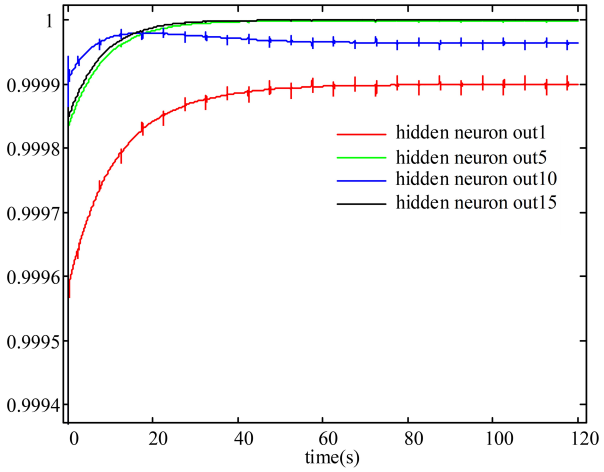

(d) Neural network hidden layer output.

Fig. 8. Simulation results.

Table 4. Errors comparison.

Item	Error range/rad
Without friction model	$(-0.0029, 0.0028)$
With friction model	$(-0.0012, 0.0012)$

Table 5. Error of trajectory changed.

Item	Error (10^{-3} rad)	RMSE/rad
Frequency change	$(-0.89, 1.4)$	4.014×10^{-4}
Amplitude change	$(-0.61, 1.3)$	2.999×10^{-4}

ing the trajectory frequency including the tracking result in Fig. 12(a), RBFNN output in Fig. 12(b) and the error curve after 82.5 s in Fig. 12(c), and the ideal tracking signal is changed from $0.35\sin(0.2\pi t)$ rad to $0.35\sin(0.125\pi(t+1.5))$ rad at 82.5 s. Fig. 13 shows the experiment of changing the trajectory amplitude including the tracking result in Fig. 13(a), RBFNN output in Fig. 13(b) and the error curve after 82.5 s in Fig. 13(c), and the ideal tracking signal is changed from $0.35\sin(0.2\pi t)$ rad to $0.175\sin(0.2\pi t)+0.175$ rad at 82.5 s. Moreover, the RMSE values are given in Table 5.

Through observing Fig. 12, Fig. 13, and Table 5, the change of target trajectory frequency and amplitude will not affect joint tracking performance.

Finally, the experiment of changing the load is carried out. And the external loads are added in the form of step. At 80 s, we add the 3 Nm step load to the manipulator joint system. The experimental results are shown in Fig. 14.

Through Fig. 14(a), we can see that the tracking performance is not affected by the additional load. And, it can be seen from Fig. 14(b) that the neural network can respond quickly and maintain the stability of the system when an external load is added in the step form. The external load is mainly compensated by the neural net-

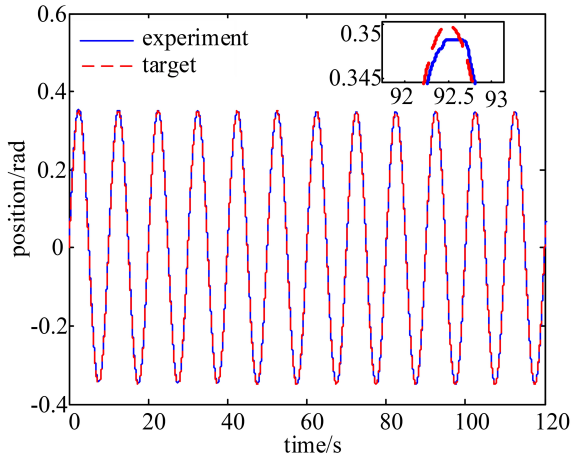

(a) Trajectory chart.

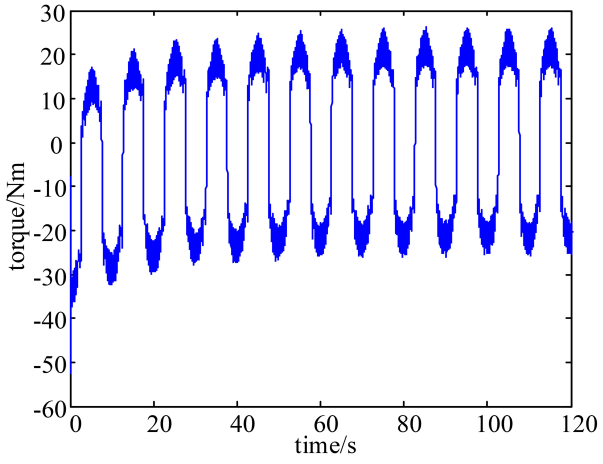

(b) RBFNN output.

Fig. 9. The experimental results without friction model.

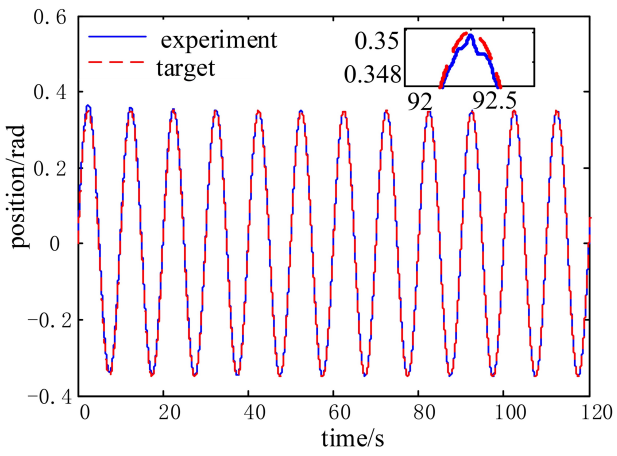

(a) Trajectory chart.

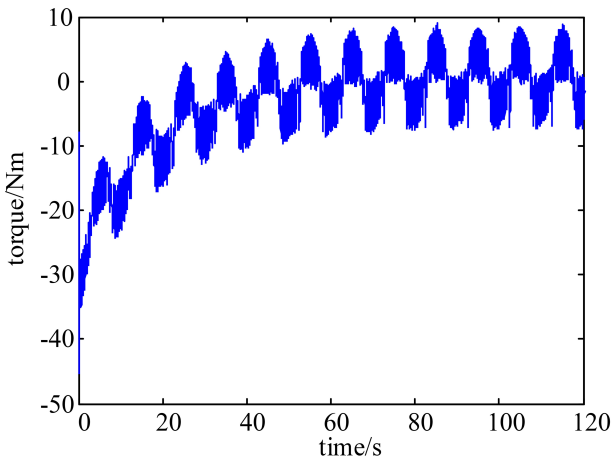

(b) RBFNN output.

Fig. 10. The experimental results with friction model.

work. Therefore, it illustrates that the introduced neural network method has good compensation performance and anti-interference ability for the manipulator joint system. Besides, Fig. 14(c) shows the tracking error after 80 s, and the range is $(-0.0008, 0.0014)$ rad and the RMSE is 4×10^{-4} rad.

Through above comparative experiments, we can obtain that the adaptive RBFNN compensation computed-torque control with friction model has good trajectory tracking performance. Compared with the controller without friction model, the trajectory tracking error is reduced by more than 50%. And, the change of the target trajectory and the external load will not decrease the tracking performance of the system due to the introduced neural network method. The neural network method makes the joint system have better compensation performance and anti-interference ability, though it may increase the convergence time.

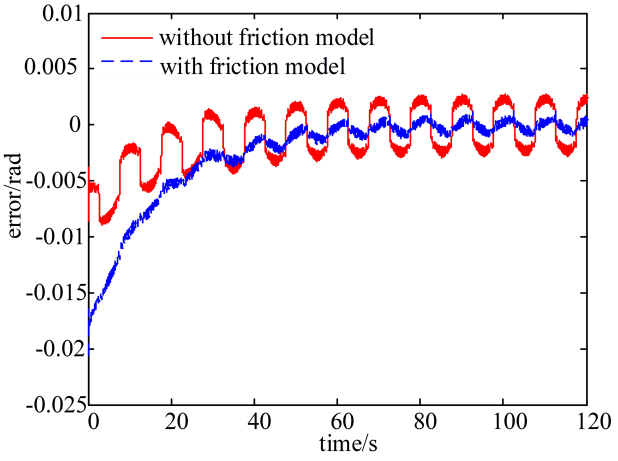

Fig. 11. Trajectory error comparison chart.

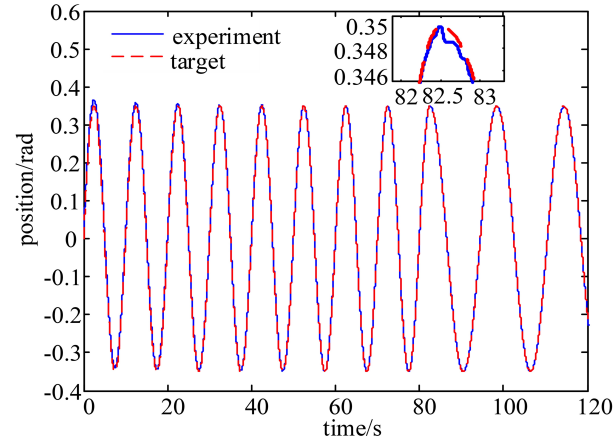

(a) Trajectory.

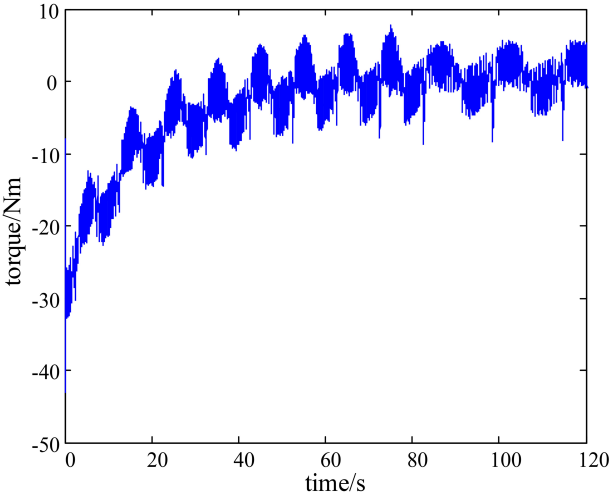

(b) RBFNN output.

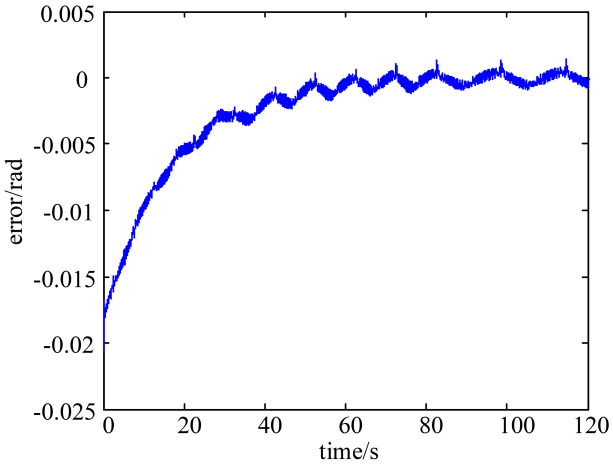

(c) Trajectory error.

Fig. 12. Trajectory frequency change.

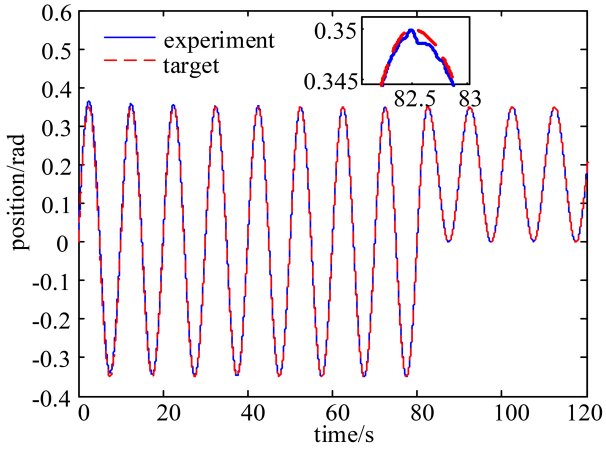

(a) Trajectory.

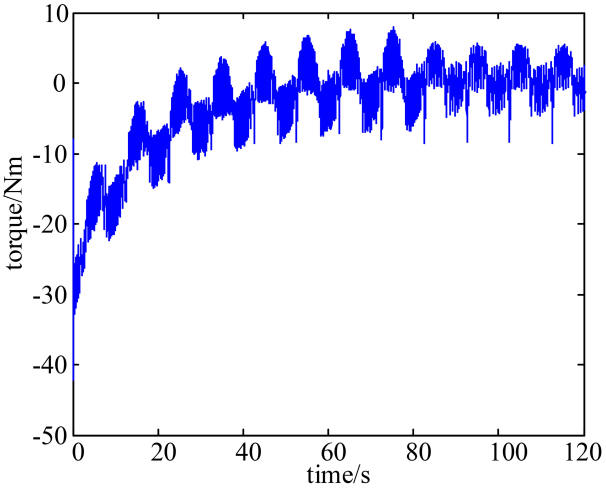

(b) RBFNN output.

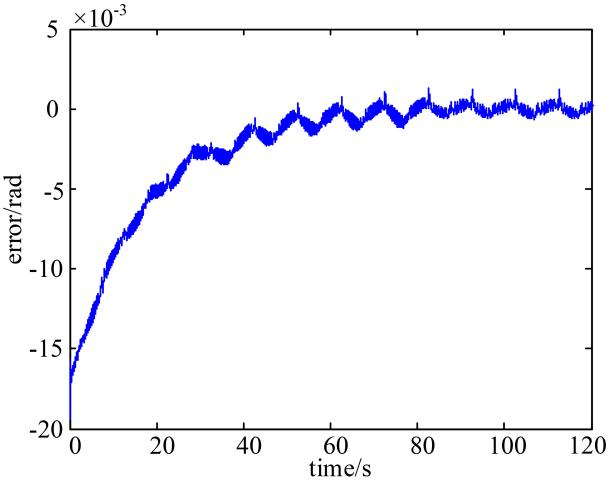

(c) Trajectory error.

Fig. 13. Trajectory amplitude change.

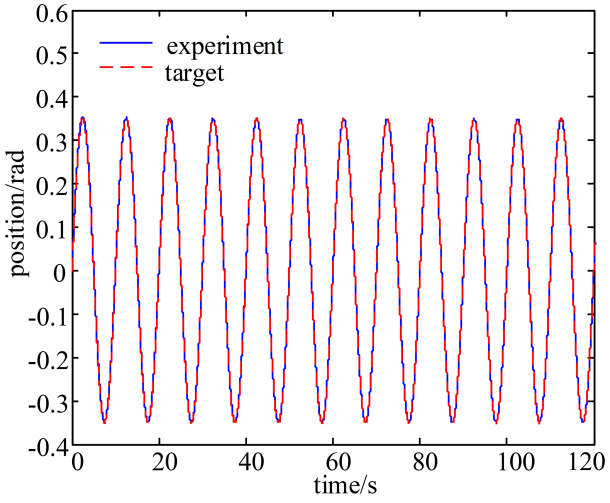

(a) Trajectory.

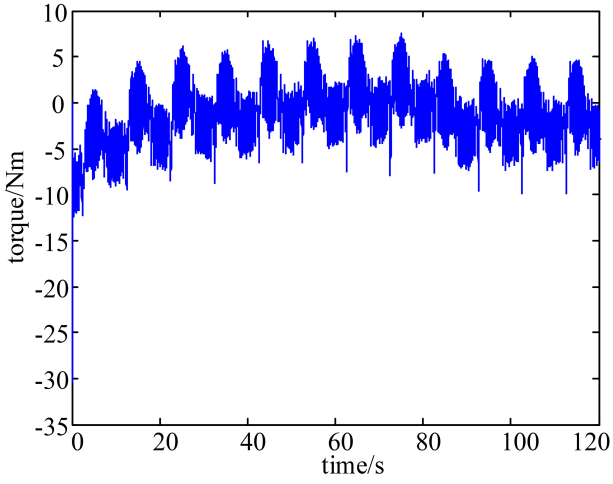

(b) RBFNN output.

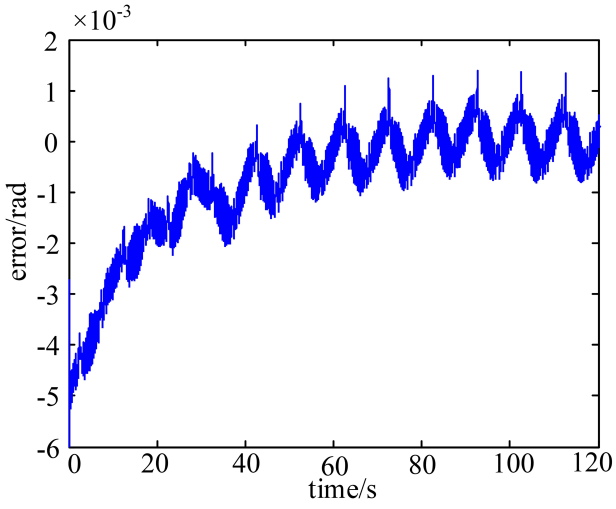

(c) Trajectory error.

Fig. 14. Load change.

5. CONCLUSIONS

In this paper, a multi-stage Stribeck friction model combined with cubic polynomial is established for the nonlinear friction in the manipulator joint, and the PSO algorithm is used to identify the parameters in the proposed friction model. Then, based on the manipulator joint dynamic model with friction model and unmodeled dynamics, the adaptive RBFNN compensation computed-torque controller is designed to realize joint angle trajectory tracking. In addition, the results of simulation experiment and contrastive experiments based on the self-developed joint can demonstrate that the joint dynamic model with the proposed friction model in this paper can effectively reduce the tracking error and improve the tracking accuracy. Especially, the multi-stage Stribeck friction model combined with cubic polynomial has higher fitting accuracy than using Stribeck model only. And the change of target trajectory and load will not affect the tracking performance based on the adaptive RBFNN compensation computed-torque controller, which is useful in practical engineering. For the next work, we will consider enhance the research results to the multi-DOF manipulator and a multi parameter adaptive adjustment of the neural network controller can be designed.

REFERENCES

[1] J. B. Méndez, C. Perez-Vidal, J. V. Segura Heras, and J. J. Pérez-Hernéndez, "Robotic pick-and-place time optimization: Application to footwear production," *IEEE Access*, vol. 8, pp. 209428-209440, 2020.

[2] A. D. Smith, J. Chapin, P. V. Birinyi, P. V. Bhagvath, and A. F. Hall, "Automated polyaxial screw placement using a commercial-robot-based, image-guided spine surgery system," *IEEE Transactions on Medical Robotics and Bionics*, vol. 3, no. 1, pp. 74-84, 2021.

[3] D. Choi, S. H. Kim, W. Lee, S. Kang, and K. Kim, "Development and preclinical trials of a surgical robot system for endoscopic endonasal transsphenoidal surgery," *International Journal of Control, Automation, and Systems*, vol. 19, pp. 1352-1362, 2021.

[4] L. Baccelliere, N. Kashiri, L. Muratore, A. Laurenzi, M. Kamedula, A. Margan, S. Cordasco, J. Malzahn, and N. G. Tsagarakis, "Development of a human size and strength compliant bi-manual platform for realistic heavy manipulation tasks," *Proc. of IEEE/RSJ International Conference on Intelligent Robots and Systems (IROS)*, pp. 5594-5601, 2017.

[5] A. Albu-Schffer, S. Haddadin, C. Ott, A. Stemmer, T. Wimboeck, and G. Hirzinger, "The DLR lightweight robot-design and control concepts for robots in human environments," *Industrial Robot*, vol. 34, no. 5, pp. 376-385, 2007.

[6] H. Nakamura, K. Ohishi, Y. Yokokura, T. Miyazaki, and A. Tsukamoto, "Fine force control without force sensor based

on reaction force estimation system considering static friction and kinetic friction," *Proc. of IECON 2016-42nd Annual Conference of the IEEE Industrial Electronics Society*, pp. 5076-5081, 2016.

[7] H. Iqbal and B. J. Yi, "Design and experimental verification of a 3-DOF spherical electromagnetic brake for haptic interface," *International Journal of Control, Automation, and Systems*, vol. 18, pp. 1299-1309, 2020.

[8] W. Wei, H. Dourra, and G. G. Zhu, "Adaptive transfer case clutch touchpoint estimation with a modified friction model," *IEEE/ASME Transactions on Mechatronics*, vol. 25, no. 4, pp. 2000-2008, 2020.

[9] K. Morito, J. Tsunoda, S. Sakaino, and T. Tsuji, "Reaction force observer using load dependent friction model," *Proc. of IEEE 15th International Workshop on Advanced Motion Control (AMC)*, pp. 423-428, 2018.

[10] H. Feng, W. H. Qiao, C. B. Yin, H. F. Yu, and D. H. Cao, "Identification and compensation of non-linear friction for an electro-hydraulic system," *Mechanism and Machine Theory*, vol. 141, pp. 1-13, 2019.

[11] R. Kelly, J. Sandoval, and V. Santibáñez, "A GUAS joint position tracking controller of torque-driven robot manipulators influenced by dynamic Dahl friction: Theory and experiments," *IEEE Transactions on Control Systems Technology*, vol. 29, no. 5, pp. 1877-1890, 2021.

[12] X. Tan, G. P. Chen, and H. B. Shao, "Modeling and analysis of spatial flexible mechanical systems with a spherical clearance joint based on the LuGre friction model," *Journal of Computational and Nonlinear Dynamics*, vol. 15, no. 1, p. 011005, 2020.

[13] L. Wang, Y. Chang, and H. T. Zhu, "Internal model control and experimental study of ankle rehabilitation robot," *Robotica*, vol. 38, no.5, pp. 940-956, 2020.

[14] S. C, Zhen, Z. Y. Zhao, X. L. Liu, F. Chen, H. Zhao, and Y. H. Chen, "A novel practical robust control inheriting PID for SCARA robot," *IEEE Access*, vol. 8, pp. 227409-227419, 2020.

[15] X. Tan, G. P. Chen, D. Y. Sun, and Y. Chen, "Dynamic analysis of planar mechanical systems with clearance joint based on LuGre friction model," *Journal of Computational and Nonlinear Dynamics*, vol. 13, no. 6, p. 061003, 2018.

[16] M. N. Nevmerzhitskiy, B. S. Notkin, A. V. Vara, and K. V. Zmeu, "Friction model of industrial robot joint with temperature correction by example of KUKA KR10," *Journal of Robotics*, vol. 2019, pp. 1-11, 2019.

[17] H. Guo, B. Zhou, P. Yang, and X. Gu, "Application of modified Stribeck model and simulated annealing genetic algorithm in friction parameter identification," *Proc. of 12th International Conference on Intelligent Systems and Knowledge Engineering (ISKE)*, pp. 1-5, 2017.

[18] C. Lin, H. Yau, and Y. Tian, "Identification and compensation of nonlinear friction characteristics and precision control for a linear motor stage," *IEEE/ASME Transactions on Mechatronics*, vol. 18, no. 4, pp. 1385-1396, May 2013.

[19] V. Sankardoss and P. Geethanjali, "PMDC motor parameter estimation using bio-inspired optimization algorithms," *IEEE Access*, vol. 5, pp. 11244-11254, March 2017.

[20] N. K. Chaturvedi and L. B. Prasad, "A comparison of computed torque control and sliding mode control for a three link robot manipulator," *Proc. of International Conference on Computing, Power and Communication Technologies (GUCON)*, pp. 1019-1024, 2018.

[21] E. Rastogi and L. B. Prasad, "Comparative performance analysis of PD/PID computed torque control, filtered error approximation based control and NN control for a robot manipulator," *Proc. of IEEE UP Section Conference on Electrical Computer and Electronics (UPCON)*, pp. 1-6, 2015.

[22] J. H. Li, J. Z. Wang, S. K. Wang, W. Qi, L. B. Zhang, Y. B. Hu, and H. Su, "Neural approximation-based model predictive tracking control of non-holonomic wheel-legged robots," *International Journal of Control, Automation, and Systems*, vol. 19, pp. 372-381, 2021.

[23] A. Nandi, B. Pradhan, N. B. Hui, D. S. Roy, and J. J. Rodrigues, "A novel hybrid neural network-based multirobot path planning with motion coordination," *IEEE Transactions on Vehicular Technology*, vol. 69, no. 2, pp. 1319-1327, 2020.

[24] H. Liu, Y. P. Pan, J. D. Cao, H. X. Wang, and Y. Zhou, "Adaptive neural network backstepping control of fractional-order nonlinear systems with actuator faults," *IEEE Transactions on Neural Networks and Learning Systems*, vol. 31, no. 12, pp. 5166-5177, 2020.

[25] J. Jiang, S. Cao, and Y. Dai, "Research on RBF neural network model compensation and adaptive control of robot manipulators," *Proc. of Chinese Control and Decision Conference (CCDC)*, IEEE, pp. 516-520, 2016.

[26] M. M. Ferdaus, M. Pratama, S. G. Anavatti, M. A. Garratt, and Y. P. Pan, "Generic evolving self-organizing neuro-fuzzy control of bio-inspired unmanned aerial vehicles," *IEEE Transactions on Fuzzy Systems*, vol. 28 , no. 8, pp. 1542-1556, 2020.

[27] Q. Jia, L. Wu, and H. Li, "Robust actuator fault reconstruction for Takagi-Sugeno fuzzy systems with time-varying delays via a synthesized learning and Luenberger observer," *International Journal of Control, Automation, and Systems*, vol. 19, pp. 799-809, 2021.

[28] K. Eltag and B. Y. Zhang, "Design robust self-tuning FPIDF controller for AVR system," *International Journal of Control, Automation, and Systems*, vol. 19, pp. 910-920, 2021.

[29] C. H. Wang, Y. Wan, and X. C. Liang, "Model establishment with Stribeck friction and fuzzy PID control for Cartesian picking robot system," *Proc. of Chinese Automation Congress (CAC)*, IEEE, pp. 3070-3074, 2017.

[30] W. Sun, J. W. Lin, S. F. Su, N. Wang, and M. J. Er, "Reduced adaptive fuzzy decoupling control for lower limb exoskeleton," *IEEE Transactions on Cybernetics*, vol. 51, no. 3, pp. 1099-1109, 2021.

[31] W. Sun, S. F. Su, J. W. Xia, and Y. Q. Wu, "Adaptive tracking control of wheeled inverted pendulums with periodic disturbances," *IEEE Transactions on Cybernetics*, vol. 50, no. 5, pp. 1867-1876, 2020.

[32] Z. Anjum and Y. Guo, "Finite time fractional-order adaptive backstepping fault tolerant control of robotic manipulator," *International Journal of Control, Automation, and Systems*, vol. 19, pp. 301-310, August 2021.

[33] C. Zou, T. Tao, G. D. Jiang, X. S. Mei, and J. H. Wu, "A harmonic drive model considering geometry and internal interaction," *Proceedings of the Institution of Mechanical Engineers, Part C: Journal of Mechanical Engineering Science*, vol. 231, no. 4, pp. 728-743, 2017.

[34] W. W. Shang, C. Shuang, and G. Yuan, "Adaptive computed torque control for a parallel manipulator with redundant," *Robotica*, vol. 30, pp. 457-466, May 2012.

Xiaobin Shen received his M.S. degree in China Jiliang University in 2020. His research interests include design of modular robot joint and joint torque control.

Kun Zhou received his Ph.D. degree in the School of Electrical Engineering at Southwest Jiaotong University in 2018. He is currently a lecturer in the College of Mechanical and Electrical Engineering at China Jiliang University, China. His research interests include intelligent control algorithm, delayed neural networks, and fuzzy control and applications.

Rui Yu received her B.S. and M.S. degrees in China Jiliang University, in 2017 and 2020, respectively. She is currently pursuing a Ph.D. degree in control science and engineering, TongJi University. Her research interests include adaptive control, nonlinear system, and multi-agents control.

Binrui Wang received his Ph.D. degree in pattern recognition and intelligent system from the School of Information Science and Engineering at Northeastern University in 2005. Currently, he is a professor in the College of Mechanical and Electrical Engineering at China Jiliang University, PRC. His research interests include intelligent control algorithm and humanoid robot.